

Effects of 3,4-dihydroxyphenyl groups in water-soluble phospholipid polymer on stable surface modification of titanium alloy

Ye Yao^{a,c}, Kyoko Fukazawa^a, Nan Huang^c, Kazuhiko Ishihara^{a,b,*}

^a Department of Materials Engineering, The University of Tokyo, 7-3-1, Hongo, Bunkyo-ku, Tokyo 113-8656, Japan

^b Department of Bioengineering, The University of Tokyo, 7-3-1, Hongo, Bunkyo-ku, Tokyo 113-8656, Japan

^c Department of Materials Science and Technology, Southwest Jiaotong University, Chengdu, Sichuan, China

ARTICLE INFO

Article history:

Received 21 April 2011

Accepted 24 June 2011

Available online 18 July 2011

Keywords:

Surface modification

Phospholipid polymer

3,4-dihydroxyphenyl groups

Titanium alloy substrate

Reduced biofouling

ABSTRACT

The surface of a titanium (Ti) alloy substrate was modified by a simple and quick process using a water-soluble polymer, and the effects of 3,4-dihydroxyphenyl (DHP) groups in the polymer side chain on the modification process were examined. The polymers (PMDP) composed of both 2-methacryloyloxyethyl phosphorylcholine (MPC) unit and 3,4-dihydroxyphenyl methacrylate unit were synthesized for surface anchoring. The Ti alloy substrate was coated with PMDP using an aqueous solution of the polymer. A PMDP layer with a thickness of 20 nm was formed on the Ti alloy substrate simply by dip coating for 10 s without drying. Even when the Ti alloy substrate with PMDP coating was immersed in the aqueous medium for 1 week, no change in the thickness was observed, i.e., the PMDP layer was bound to the surface very stably. Oxidation of the DHP groups reduced the stability of the polymer layer significantly. Thus, the DHP groups play a significant role in achieving stable binding. Protein was adsorbed on the Ti alloy substrate; however, this was not observed for the PMDP-coated Ti alloy substrate. In conclusion, we confirmed the effects of DHP groups in PMDP on the stability of the coating on the Ti alloy substrate. Moreover, we found that surface treatment using PMDP was simple, quick, and reliable, and thus, it has great potential for improving biofouling of Ti alloy substrates used in medical devices.

© 2011 Elsevier B.V. All rights reserved.

1. Introduction

Titanium (Ti) alloys have many desirable properties such as a relatively low Young's modulus, good fatigue strength, formability, machinability, and corrosion resistance. Accordingly, they have been widely used in biomedical devices and components since the late 1970s, especially in cardiac and cardiovascular applications (e.g., prosthetic heart valves, protective cases in pacemakers, implantable blood pumps, cardiovascular stents, and circulatory devices) [1]. However, Ti alloy substrates induce severe biological responses such as thrombus formation and tissue reaction [2]. As a result, anticoagulant therapy is necessary to minimize the risk of thromboembolic complications. Therefore, surface modification of Ti alloy substrates is indispensable for improving its thrombogenicity and tissue compatibility.

Protein adsorption is the first essential event followed by biological responses such as acute thrombus formation and inflammation

and then fibrous encapsulation, bacterial adhesion, and infection [3]. It is generally believed that reducing protein adsorption on the substrates can significantly attenuate these adverse biological responses. One well-known polymeric material used to prevent protein adsorption is hydrophilic poly(ethylene glycol) (PEG) [4]. Indeed, PEG functions well under both *in vitro* and *in vivo* conditions for a relatively short period. However, because PEG-based materials are susceptible to degradation by spontaneous oxidation under physiological conditions, these systems lack long-term stability, which reduces their effectiveness as a surface modifier [5]. In other words, PEG-based materials are not suitable for use in implantable cardiovascular devices.

Another promising and effective way of preventing protein adsorption to attain biocompatibility is to prepare an artificial cell membrane surface on the substrates using phospholipid polymers. Such polymers have been synthesized using 2-methacryloyloxyethyl phosphorylcholine (MPC), which is a methacrylate monomer bearing the same polar group as that in the natural phospholipid molecules in the side chain [6,7]. Ishihara et al. developed a synthetic route for MPC in 1989 that has been successfully applied worldwide. MPC polymers show adequate stability both chemically and physically even when under *in vivo* conditions. Moreover, they have excellent thrombogenicity and tissue

* Corresponding author at: The University of Tokyo, Department of Materials Engineering, 7-3-1, Hongo, Bunkyo-ku, Tokyo, 113-8656, Japan.
Tel.: +81 3 5841 7124; fax: +81 3 5841 8647.

E-mail address: ishihara@mpc.t.u-tokyo.ac.jp (K. Ishihara).

compatibility [8–12]. At present, MPC polymers are widely used for the surface modification of implantable medical devices and artificial organs [13–17].

There are many reports of surface immobilization of MPC polymers on Ti alloy substrates. However, these methods have many limitations for widespread practical use. Layer-by-layer assembly (LBL) involves complex multistep procedures [18], the self-assembled monolayer (SAMs) technique requires surface-specific interaction [19], and surface-initiated atom transfer radical polymerization (ATRP) needs unstable polymerization conditions [20]. Poly(MPC-co-*n*-butyl methacrylate (BMA)) (PMB) is a typical MPC polymer. The polymer suppresses non-specific protein adsorption, platelet adhesion, activation, and aggregation in whole blood, even in the absence of anticoagulants [8–11,21]. The coating procedure of PMB from its solution is relatively simple [8–10,16]. PMB can be tightly bound to the substrate by the drying process. More than 5 h of prehydration time is needed to enable the surface functionalities of PMB, although the time depends on the thickness of the PMB layer [22]. However, this prehydration process cannot be applied to medical devices such as cardiovascular stents and blood separation devices. Thus, for practical applications, it is desirable to use a more simple, convenient, and versatile method to immobilize MPC on Ti alloy substrate surface without prehydration.

Recently, to facilitate convenient adhesion of organic compounds to metal substrates, mussel-inspired chemistry has been widely investigated [23–25]. Mussels can rapidly and permanently adhere to all types of inorganic and organic wet surfaces in aqueous environments. Such adhesive properties rely on the repeated 3,4-dihydroxy-L-phenylalanine (DOPA) motif found in the foot protein of mussels [26]. Although the exact mechanism of adhesion is not fully understood, it has been widely speculated that the 3,4-dihydroxyphenyl (DHP) group of DOPA is responsible for the adhesion [27,28]. Lee [29] reported that the oxidation of the DOPA motif in the foot proteins dramatically reduces the strength of adhesion to metals. This mussel-inspired chemistry can be used for surface modification using polymers. When a polymer with DHP groups is in contact with a metal substrate, the thin polymer film is spontaneously deposited on the surface. The functionalization of the polymers imparts new characteristics to the metal substrate. In fact, it has been reported that PEG with DHP groups was used to modify a TiO₂ surface in the pH range 6.0–7.4 to reduce protein adsorption on the surface [30].

In this study, we synthesized water-soluble MPC polymers that have DHP groups in the side chain (PMDP). Surface modification of the Ti alloy substrate was carried out using an aqueous solution of the polymer. The surface characteristics and stability of the coated polymer layer were examined, and the effects of the DHP groups on the adhesion of PMDP have been discussed. Finally, we examined the reduction of protein adsorption on the surface of the Ti alloy substrate after modification using PMDP.

2. Materials and methods

2.1. Materials

Two types of water-soluble MPC polymer, poly(MPC-co-methacrylic acid (MAA)) (PMA), were obtained from NOF Co. (Tokyo, Japan) which were synthesized by conventional radical polymerization of MPC and MAA [31]. The compositions of the MPC units in PMA were 30 unit mol% (denoted PMA3) and 50 unit mol% (denoted PMA5). The number average molecular weight (*M_n*) of PMA3 and PMA5 was 2.7×10^5 and 3.2×10^5 , respectively. Dopamine hydrochloride was purchased from Sigma–Aldrich (St. Louis, MO, USA). 1-Ethyl-3-(3-dimethylaminopropyl)carbodiimide, hydrochloride (WSC) was purchased

from Dojindo (Kumamoto, Japan). A Ti alloy substrate with thickness of 1.0 mm was purchased from Sumitomo Metals, Ltd. (Tokyo, Japan). The Ti alloy substrate was cut into 10 mm × 10 mm pieces and polished with #2000 and #3000 polish papers. The pieces were then rinsed in acetone and ethanol by sonication for 15 min. After drying in air, the substrates were cleaned using oxygen plasma apparatus (PR500 plasma reactor, Yamato Science, Tokyo, Japan) for 10 min before use. To test the resistance of the substrate surface to protein adsorption, bovine serum albumin (BSA, Sigma–Aldrich) was used without further purification.

2.2. Synthesis of phospholipid polymer

The water-soluble MPC polymer with DHP groups was synthesized by condensation reaction between PMA and dopamine hydrochloride. The reaction scheme is shown in Fig. 1. Dopamine hydrochloride and WSC were dissolved in 4 mL of PMA aqueous solution (5.0 wt%), and 96 mL of pH 6.0 buffered solution (potassium dihydrogen phosphate and sodium hydroxide) was added. The reaction was carried out at room temperature for 24 h under Ar gas atmosphere to prevent the oxidation of the DHP groups. The molar ratio [dopamine hydrochloride]/[COOH] was 2.0. After the reaction, the polymer solution was filtered using ultrafiltration membranes (Millipore Co., USA; molecular size cut off: 3.0×10^4) until there was no further release of unreacted dopamine through the membrane, which was confirmed by ultraviolet (UV, V-560, Jasco Co., Tokyo, Japan) adsorption. The polymer solution was freeze-dried. PMDP prepared from PMA3 are denoted as PMDP3, and that prepared from PMA5 are denoted as PMDP5. The chemical structure of these polymers was confirmed by both UV and Fourier transform infrared (FTIR) spectroscopy (FT/IR-615, Jasco) for 32 scans over the range 650–4000 cm⁻¹ at a resolution of 4.0 cm⁻¹. The contents of the DHP groups in PMDP were calculated from the UV absorbance of the polymer aqueous solution at 280 nm by comparing with that of a given concentration of dopamine hydrochloride.

2.3. Surface modification on Ti alloy substrate with PMDP

The PMDP solution was prepared using the following aqueous media: pure water (pH about 5.5) and buffered solutions with pH 6.0 and 8.5. The Ti alloy substrate was coated with the PMDE solution by simply dipping it in the solution at room temperature for either 10 s or 24 h.

The surface of the substrate was analyzed by FTIR reflection adsorption spectroscopy to confirm that the substrate coated with the solution. The surface morphology was then observed using an atomic force microscope (AFM, Nihon Veeco, Tokyo, Japan) operated in the tapping mode. The measurements were performed under ambient conditions using a standard cantilever at a scan rate of 1.0 Hz. The root mean square (RMS) surface roughness was calculated from the roughness profiles.

Following the polymer adhesion process, a quartz crystal microbalance (QCM) sensor was used with dissipation monitoring (QCM-D, Q-Sense, Gothenburg, Sweden) and a fundamental resonant frequency of 5.0 MHz. The QCM is widely used to measure the change in mass (Δm) of materials/molecules attached to the surface of the QCM sensor via changes in the resonant frequency (Δf). The QCM-D can detect adsorbed mass up to a resolution of less than a few nanograms per square centimeter. The resonant frequency of the QCM sensor (*f*) depends on the total oscillating mass. When a thin film is attached to the QCM sensor, the frequency decreases; if the film is thin and rigid, the decrease in frequency is proportional to the mass of the film. Thus, the amount of the adsorbed material on a given surface can be measured by the decrease in the frequency of the oscillator. In this manner, the QCM operates as a very sensitive balance. The mass of the adhered layer can be calcu-

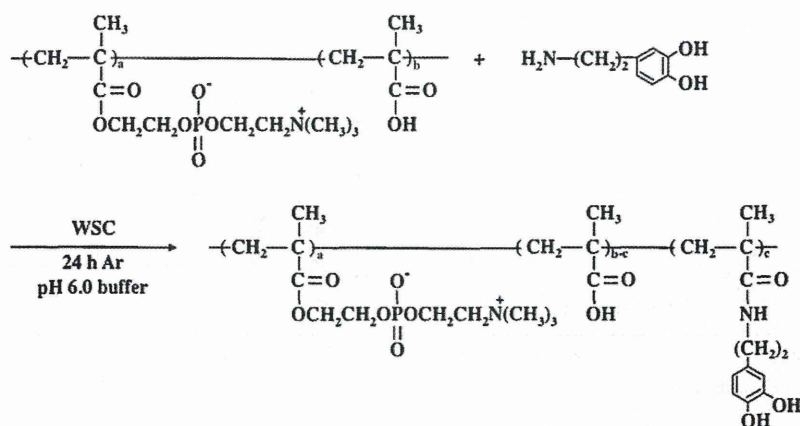


Fig. 1. Synthetic route of PMDP.

lated using the Sauerbrey equation [32], $\Delta m = -C \times \Delta f n / n$, where $C = 17.7 \text{ ng cm}^{-2} \text{ Hz}^{-1}$, n is the overtone number ($n = 1, 3, 5, 7$), and $f n$ is the frequency of the overtone. Four resonant frequencies (overtones, $n = 1, 3, 5$, and 7) were used to detect the oscillation of the shearwave through the crystal at 5, 15, 25, and 35 MHz, respectively. The data from the seventh overtone is reported, because it contained minimum noise. The Ti-coated (Ti/Au) QCM sensor obtained from Q-Sense was cleaned using oxygen plasma for 10 min before use. The QCM sensor was exposed to the water solution until a stable baseline of the QCM signals was obtained. The QCM cell was then filled with 2.0 mg mL^{-1} of PMDP aqueous solution. After the PMDP solution was retained for 20 min in the QCM cell, phosphate buffered saline (PBS) solution was flowed to replace the PMDP solution and wash away the weakly adsorbed PMDP from the surface. The QCM signals were monitored throughout the procedure. All the measurements were performed at 37°C and repeated at least three times.

2.4. Surface characterization and stability evaluation of the coating polymer layer

After coating, the Ti alloy substrates were immersed in water at room temperature for at least 2 days to evaluate the stability of the coating polymer layer. The hydrophilicity of the Ti alloy substrates before and after immersion in the PMDP solution was evaluated with a contact angle goniometer (CA-W, Kyowa Co. Ltd., Tokyo, Japan). The captive-bubble method was used to determine the static contact angle. Each Ti alloy substrate was immersed in water to equilibrate and then fixed horizontally on a metal plate. A small air bubble was attached to the surface of the Ti alloy substrates. The measurement was repeated five times for each substrate, and the average was calculated.

The thickness of the PMDP layer formed on the substrate was measured using an ellipsometer (J. A. Woollam Co., Inc., Tokyo, Japan) at an incident angle of 70° in the visible region. The thickness of the polymer coating layer was determined using a Cauchy layer model with an assumed refractive index of 1.49 at 632.8 nm.

A surface elemental analysis was carried out using an X-ray photoelectron spectroscope (XPS, AXIS-HSi165, Kratos/Shimadzu Co., Kyoto, Japan) with 15 kV Al $K\alpha$ radiation source at the anode. The applied voltage was 15 kV, and the electric current was 10 mA. The take-off angle of the photoelectrons was maintained at 90° .

To examine the effects of oxidation of the DHP groups in PMDP, the PMDP aqueous solution was kept in air for spontaneous oxidation. After one month, the solution was freeze-dried, and the chemical structure of the remaining polymer was analyzed by both UV and FTIR spectroscopy. The polymer was dissolved in water

again, and the solution was used for coating the Ti alloy substrate. The stability of the polymer layer was evaluated by ellipsometry.

2.5. Measurement of amount of protein adsorbed on Ti alloy substrate

The amount of BSA adsorbed on the PMDP3-coated surface was quantified using the QCM-D. First, a Ti-coated QCM sensor was used as a QCM-D. After flowing 2.0 mg mL^{-1} of PMDP3 aqueous solution through the QCM cell, the sensor was exposed to a PBS (pH 7.4) solution until a stable baseline of QCM signals was obtained. Then, 1.0 mg mL^{-1} of BSA in PBS was flowed to fill the QCM cell. After the BSA solution was retained for 20 min in the QCM cell, the PBS solution was flowed to replace the BSA solution and wash away the weakly adsorbed BSA from the surface. The QCM signals were monitored throughout the procedure. All the measurements were performed at 37°C and repeated at least three times.

3. Results and discussion

3.1. Characterization of PMDP

We considered that the DHP groups were useful for binding the polymer after adsorption on the Ti alloy substrate from its aqueous solution. The IR spectra of the two PMDP polymers are shown in Fig. 2 with the starting materials, PMA and dopamine hydrochloride. The IR spectra of PMDP3 and PMDP5 were similar. The DHP group in PMDP was verified by the appearance of an absorbance

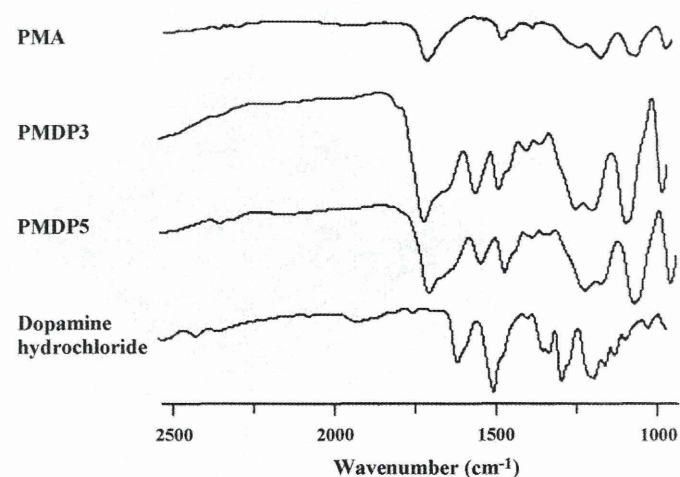


Fig. 2. IR spectra of PMA, PMDP, and dopamine hydrochloride.

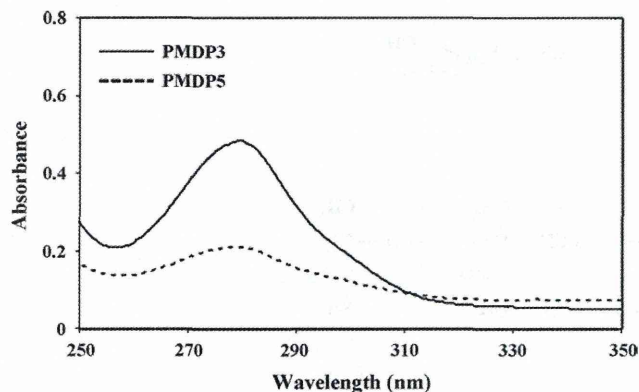


Fig. 3. UV absorption spectrum of PMDP aqueous solution (only the spectrum of PMDP3 is shown).

peak at 1553 cm^{-1} , which is attributed to the aromatic ring of dopamine hydrochloride. In addition, the presence of the ester carbonyl group of the methacrylate units in PMDP was verified by the appearance of an absorbance peak at 1715 cm^{-1} . The UV spectrum shown in Fig. 3 confirms the introduction of the DHP group in PMDP. An adsorption was observed at 280 nm , corresponding to the DHP groups. Absorbance calculations showed that the content of DHP groups was $4.0\text{ unit mol}\%$ in PMDP3 and $2.0\text{ unit mol}\%$ in PMDP5. The content of DHP groups in the polymer chain was less than expected. This was because of the solubility of dopamine hydrochloride and reactivity of carboxylate groups in PMA at this pH.

3.2. Surface modification on Ti alloy substrate with PMDP

The Ti alloy substrate was immersed in the aqueous solution of PMDP for different periods. After immersion in the PMDP solution for 10 s, the Ti alloy substrate was pulled out and dried under vacuum for observation with AFM. The AFM images are shown in Fig. 4. The RMS surface roughness of the original Ti alloy substrate was 1.0 nm , whereas that of the PMDP3-coated Ti alloy substrate was only 0.5 nm , indicating that the surface roughness can be reduced by this polymer coating process. The amount of polymer on the Ti alloy substrate was measured with QCM-D. As shown in Fig. 5, a small amount of PMA was deposited on the substrate (small change in frequency); on the other hand, 354 ng cm^{-2} of PMDP3 adhered to the substrate (20 Hz change in frequency). These results show that PMDP3 covered and adhered to the Ti alloy substrate immediately

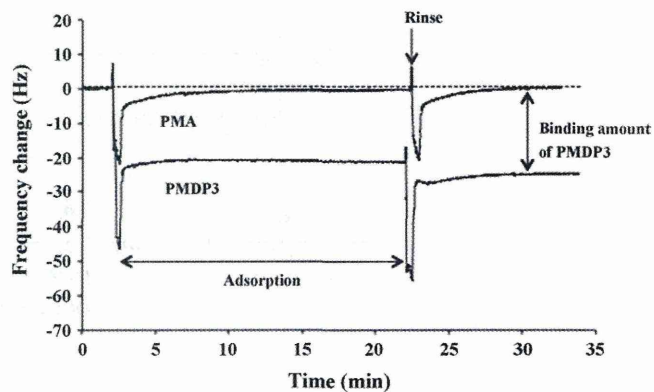


Fig. 5. Adsorption and binding process of PMDP3 and PMA3 on Ti-coated QCM sensor.

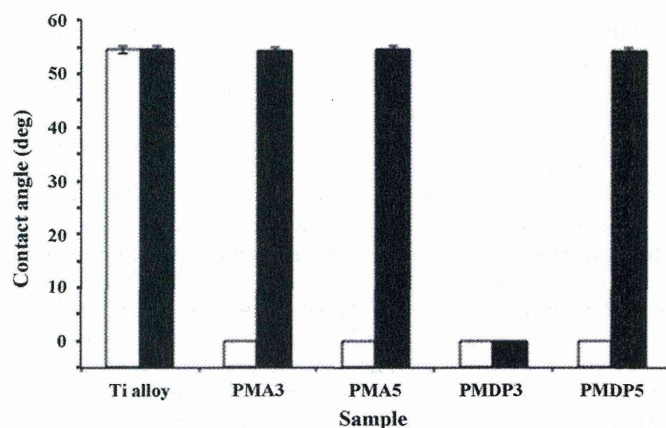


Fig. 6. Change in contact angle of Ti alloy substrate treated with PMA and PMDP by immersion in water for 2 days. Open column: Just after coating for 10 s. Closed column: After 2 days.

from its aqueous solution and formed a uniform coating layer via the dipping procedure. The peaks of DHP groups in the FTIR spectra also indicate the presence of PMDP3 on the Ti alloy substrate and ester carbonyl group after the coating procedure (data not shown).

The surface hydrophilicity was evaluated by performing contact angle measurements. PMDP is water-soluble, which means the polymer is quite hydrophilic. The contact angle was 54° on the original Ti alloy substrate, as shown in Fig. 6. After treatment

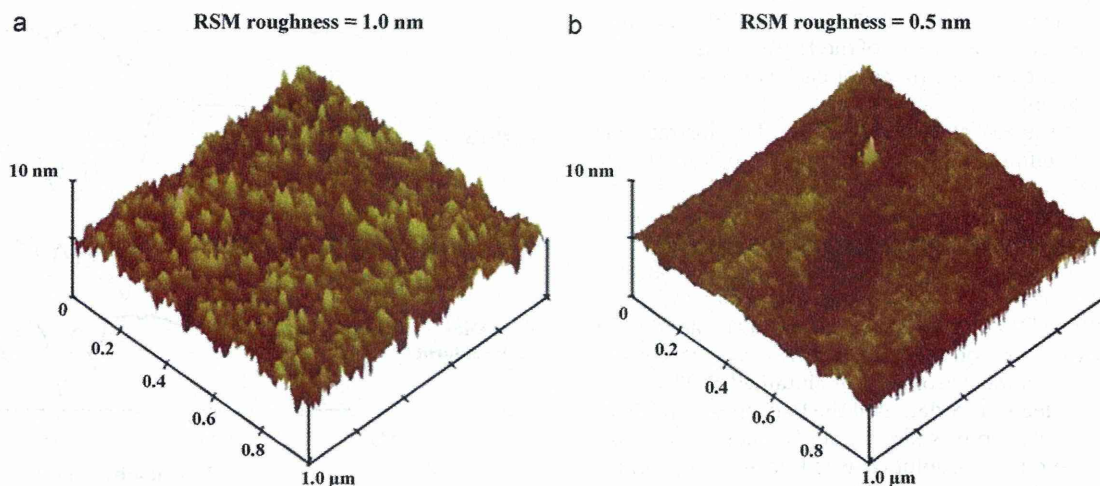


Fig. 4. AFM images of (a) original Ti alloy substrate and (b) Ti alloy substrate coated with PMDP3 by immersion for 10 s.

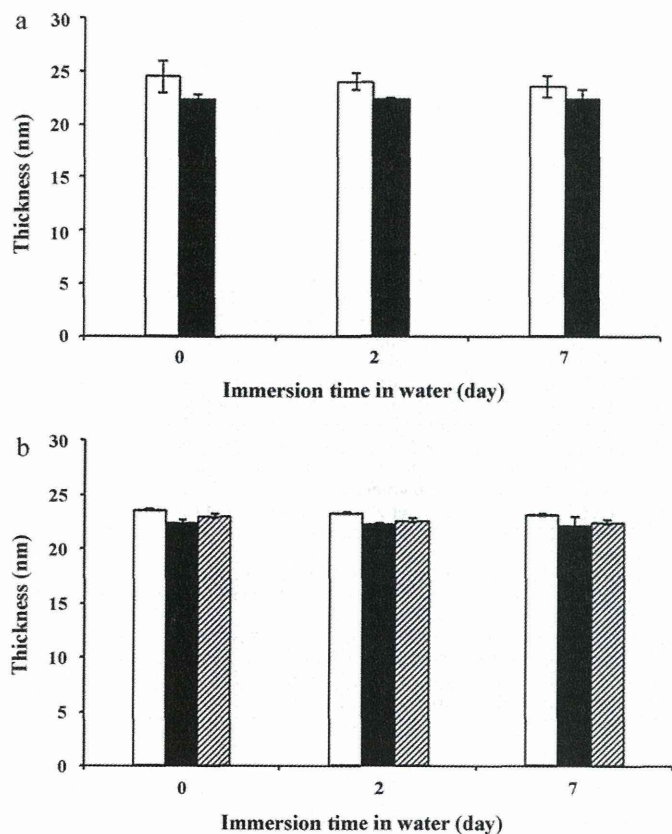


Fig. 7. Change in thickness of PMDP3 layer on Ti alloy substrate after immersion in water. (a) For different coating times (open column: 24 h; closed column: 10 s) and (b) with different pH (open column: pH 8.5 buffer; closed column: water; hatched column: pH 6.0 buffer).

with the PMDP3 solution, the contact angle decreased dramatically and reached 0° . This value was maintained even after the substrate was immersed in water for 2 days. This result suggests that PMDP3 remained on the substrate. On the other hand, in the case of PMA and PMDP5, the contact angle returned to 54° (the same as in the case of the original Ti alloy substrate) after immersion for 2 days. These polymers may be detached from the substrate. As shown in Fig. 7, the stability of the PMDP3 coating was confirmed by ellipsometry from the thickness change observed during the washing process. For both time periods (10 s and 24 h), in the case of the PMDP3 aqueous solution, the thickness of the coating layer did not change and minor differences because of the different coating periods and pH were observed. The signals of phosphorus atom at 133 eV and carbon atoms at 285–288 eV in the XPS spectra support the presence of PMDP on the Ti alloy substrate after 7 days immersion procedure (data not shown). Although the binding mechanism of the DHP group to the metal and metal oxide could not be clarified, the affinity of the DHP groups to the Ti alloy substrate was observed.

On the other hand, we considered that the reduced content of DHP groups because of oxidation may lead to instability of the polymer layer. The PMDP aqueous solution was spontaneously oxidized by air. Then, the chemical composition was studied by UV and FTIR spectroscopy. In the UV spectrum measured after oxidation, the intensity of the absorbance peak at 280 nm attributed to the aromatic ring decreased. Conversely, an IR absorbance peak appeared at 2852 cm^{-1} ; this is attributed to ketone groups. The above results confirm that the DHP groups were converted to quinone groups. The oxidized PMDP solution was used as a coating solution. As shown in Fig. 8, the thickness of the coating polymer layer changed with the washing period, and the thickness decreased within 2 days. Thus,

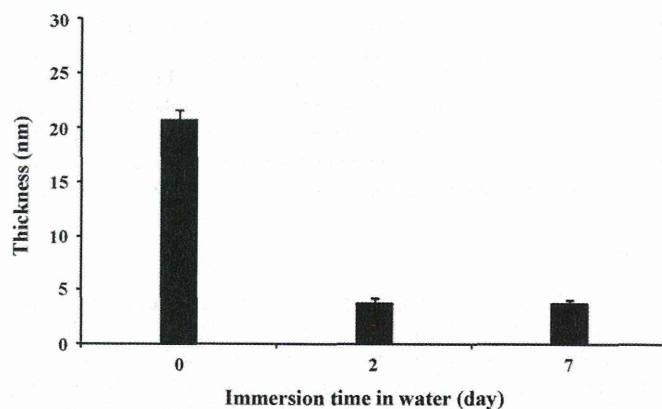


Fig. 8. Change in thickness of oxidized PMDP3 layer on Ti alloy substrate after immersion in water.

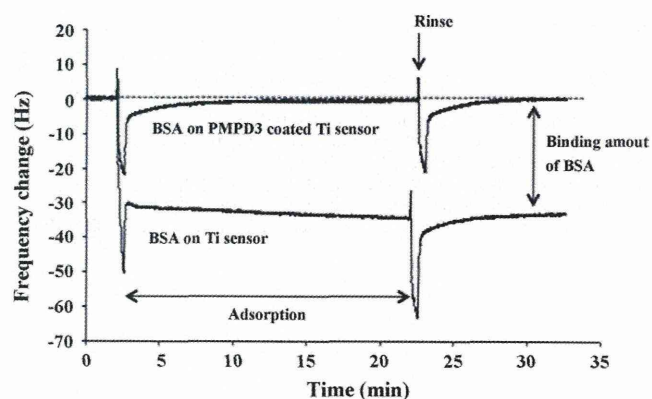


Fig. 9. Adsorption and detachment process of BSA on bare and PMDP3-modified Ti-coated QCM sensor.

the oxidation reaction weakened the binding force of the polymer on the Ti alloy substrate and caused the coating polymer layer to become unstable. These results strongly support the notion that the DHP groups in PMDP play an important role in stabilizing the coating.

3.3. Protein adsorption resistance of Ti alloy substrate treated with PMDP

Resistance to protein adsorption is one of the most important properties of biomedical materials. The effects of coating with PMDP3 were evaluated using the BSA solution. BSA is the most highly concentrated protein in blood plasma. According to the QCM signals (Fig. 9), 530 ng cm^{-2} of BSA was adsorbed on the original Ti alloy substrate (30 Hz change in frequency), whereas after treatment with PMDP3, no QCM signal because of BSA adsorption could be detected. These results indicate that the resistance to protein adsorption can be improved by coating with PMDP3. The MPC polymer gave a phosphorylcholine-group-arranged surface [22,33]. The phosphorylcholine group is electrically neutral and hydrated with free-water-like water molecules [11,34,35]. Thus, both electrostatic interaction and hydrophobic interaction are extremely weak and resistance to protein adsorption on the surface is improved [36].

4. Conclusions

A uniform layer of PMDP3 can be deposited on a Ti alloy substrate simply by dipping for 10 s in a PMDP3 aqueous solution without further treatment. The DHP groups play an important role as molecular anchors for stabilizing the binding between the coat-

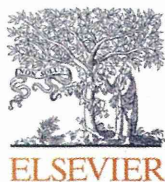
ing and the substrate. The reduction of protein adsorption on the surface treated with PMDP may induce significant suppression of biological responses, thus maintaining excellent biocompatibility of the MPC unit. In conclusion, simple and reliable surface treatment of a Ti alloy substrate was successfully carried out using bioinspired PMDP, and this method has the potential for application to high-performance cardiovascular implantable medical devices.

Acknowledgement

The authors thank Prof. Madoka Takai, Dr. Yuuki Inoue, and Dr. Ryosuke Matsuno from The University of Tokyo for the helpful discussions. This research was conducted under the CSC program in China at The University of Tokyo. One of the authors (YY) expresses her gratitude. The research was partially supported by Core Research for Evolutional Science and Technology (CREST), Japan Science and Technology Agency.

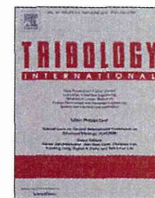
References

- [1] X. Liu, P.K. Chu, C. Ding, *Mater. Sci. Eng. R.* 47 (2004) 49.
- [2] J. Hong, J. Andersson, K. Ekdahl, et al., *Thromb. Haemost.* 82 (1999) 58.
- [3] D.G. Castner, B.D. Ratner, *Surf. Sci.* 500 (2002) 28.
- [4] C. Gao, G. Li, H. Xue, et al., *Biomaterials* 31 (2010) 1486.
- [5] C.W. McGary Jr., *J. Polym. Sci.* 46 (1960) 51.
- [6] K. Ishihara, T. Ueda, N. Nakabayashi, *Polym. J.* 22 (1990) 355.
- [7] T. Ueda, H. Oshida, K. Kurita, et al., *Polym. J.* 24 (1992) 1259.
- [8] K. Ishihara, R. Aragaki, T. Ueda, et al., *J. Biomed. Mater. Res.* 24 (1990) 1069.
- [9] K. Ishihara, N.P. Ziats, B.P. Tierney, et al., *J. Biomed. Mater. Res.* 25 (1991) 1397.
- [10] K. Ishihara, H. Oshida, T. Ueda, et al., *J. Biomed. Mater. Res.* 26 (1992) 1543.
- [11] K. Ishihara, H. Nomura, T. Mihara, et al., *J. Biomed. Mater. Res.* 39 (1998) 323.
- [12] A.L. Lewis, *Colloids Surf. B: Biointerfaces* 18 (2000) 261.
- [13] T. Yoneyama, K. Ishihara, N. Nakabayashi, et al., *J. Biomed. Mater. Res.* 43 (1998) 15.
- [14] A.L. Lewis, L.A. Tolhurst, P.W. Stratford, *Biomaterials* 23 (2002) 1697.
- [15] M. Galli, L. Sommariva, F. Prati, et al., *Catheter. Cardiovasc. Intervent.* 53 (2001) 182.
- [16] T.A. Snyder, H. Tsukui, S.I. Kihara, et al., *J. Biomed. Mater. Res. Part A* 81A (2007) 85.
- [17] T. Moro, Y. Takatori, K. Ishihara, et al., *Nat. Mater.* 3 (2004) 829.
- [18] J. Choi, T. Konno, T. Matsuno, et al., *Colloids Surf. B: Biointerfaces* 67 (2008) 216.
- [19] Y. Iwasaki, N. Saito, *Colloids Surf. B: Biointerfaces* 32 (2003) 77.
- [20] Y. Zhao, Q. Tu, J. Wang, et al., *Appl. Surf. Sci.* 257 (2010) 1596.
- [21] Y. Iwasaki, K. Ishihara, *Anal. Bioanal. Chem.* 381 (2005) 534.
- [22] A. Yamasaki, Y. Imamura, K. Kurita, *Colloid Surf. B: Biointerfaces* 28 (2003) 53.
- [23] H. Lee, S. Dellatore, W. Miller, et al., *Science* 318 (2007) 426.
- [24] K. Huang, B.P. Lee, D.R. Ingram, et al., *Biomacromolecules* 3 (2002) 397.
- [25] H. Lee, S.M. Dellatore, W.M. Miller, et al., *Science* 318 (2007) 426.
- [26] J.H. Waite, M.L. Tanzer, *Science* 212 (1981) 1038.
- [27] A.A. Ooka, R.L. Garrell, *Biopolymers* 57 (2000) 92.
- [28] M. Yu, J. Hwang, T.J. Deming, et al., *J. Am. Chem. Soc.* 121 (1999) 5825.
- [29] H. Lee, N.F. Scherer, P.B. Messersmith, et al., *Proc. Nat. Am. Sci. U.S.A.* 103 (2006) 12999.
- [30] J.L. Dalsin, L. Lin, S. Tosatti, et al., *Langmuir* 21 (2005) 640.
- [31] M. Kimura, K. Fukumoto, J. Watanabe, et al., *J. Biomater. Sci. Polym. Ed.* 15 (2004) 631.
- [32] G. Sauerbrey, *Z. Phys. A: Hadrons Nucl.* 155 (1959) 206.
- [33] S. Clarke, M.C. Davies, C.J. Roberts, et al., *Langmuir* 16 (2000) 5116.
- [34] H. Kitano, K. Sudo, K. Ichikawa, et al., *J. Phys. Chem. B* 104 (2000) 10425.
- [35] H. Kitano, M. Imai, T. Mori, et al., *Langmuir* 19 (2003) 10260.
- [36] Y. Xu, M. Takai, K. Ishihara, *Ann. Biomed. Eng.* 38 (2010) 1938.



Contents lists available at ScienceDirect

Tribology International

journal homepage: www.elsevier.com/locate/triboint

Analysis of biphasic lubrication of articular cartilage loaded by cylindrical indenter

Nobuo Sakai^{a,*}, Yuichiro Hagihara^a, Tsukasa Furusawa^a, Natsuko Hosoda^b, Yoshinori Sawae^a, Teruo Murakami^a

^a Department of Mechanical Engineering, Kyushu University, 744 Motoooka, Nishi-ku, Fukuoka 819-0395, Japan

^b Former Kyushu University, Japan

ARTICLE INFO

Article history:

Received 4 September 2010

Received in revised form

30 December 2010

Accepted 18 March 2011

Available online 8 April 2011

Keywords:

Articular cartilage

Biphasic lubrication

Finite element

Migrating contact

ABSTRACT

Combination of theoretical biphasic analyses and corresponding experimental measurements for articular cartilage has successfully revealed the fundamental material properties and time-dependent mechanical behaviors of articular cartilage containing plenty of water. The insight of load partitioning between solid and fluid phases advanced the prediction of the frictional behavior of articular cartilage. One of the recent concerns about biphasic finite element (FE) analysis seems to be a dynamic and physiological condition in terms of mechanical functionality as a load-bearing for articular joint system beyond material testing, which has mainly focused on time-dependent reaction force and deformation in relatively small and low speed compression. Recently, the biphasic FE model for reciprocating sliding motion was applied to confirm the frictional effect on the migrating contact area. The results indicated that the model of a cylindrical indenter sliding over the cartilage surface remarkably sustained the higher proportion of fluid load support than a condition without migrating contact area, but the effectiveness of constitutive material properties has not been sufficiently evaluated for sliding motion. In our present study, at the first stage, the compressive response of the articular cartilage was examined by high precision testing machine. Material properties for the biphasic FE model, which included inhomogeneous apparent Young's modulus of solid phase along depth, strain-dependent permeability and collagen reinforcement in tensile strain, were estimated in cylindrical indentation tests by the curve fitting between the experimental time-dependent behavior and FE model simulation. Then, the biphasic lubrication mechanism of the articular cartilage including migrating contact area was simulated to elucidate functionality as a load-bearing material. The results showed that the compaction effect on permeability of solid phase was functional particularly in the condition without the migrating contact area, whereas in sliding condition the compaction effect did not clearly show its role in terms of the proportion of fluid load support. The reinforcement of solid phase, which represented the collagen network in the tissue, improved the proportion of fluid load support especially in the sliding condition. Thus, a functional integration of constitutive mechanical properties as a load-bearing was evaluated by FE model simulation in this study.

© 2011 Elsevier Ltd. All rights reserved.

1. Introduction

Articular cartilage is a superior load-bearing material of diarthrodial joint in endoskeleton bodies. The cartilage layer covers bones in synovial joint to realize excellent frictional properties of prevailing over various rubbing circumstances and loads. The cartilage as a tribological material is exposed to a wide range of loads up to 10 times body weight, while relative speed between

rubbing surfaces that includes rolling and sliding motions subsides nearly stationary in activities of daily living. Upon these severe conditions, friction coefficient of synovial joint is maintained within a very low value, which normally ranges under 0.03. In normal body, frictional function of articular cartilage endures through whole life accompanying metabolic regeneration of the cartilaginous tissue. Constitution and functionality of articular cartilage complex as the biphasic lubrication material has been recently reviewed by Ateshian [1] with a conclusive statement. Katta et al. [2] presented the biotribological characteristics of articular cartilage from the viewpoint of various phenomena, which included boundary lubrication and artificial substitutions for the cartilage. In this paper, only a brief introduction of researches on mechanical functionalities of

* Corresponding author. Tel.: +81 92 802 3076; fax: +81 92 802 0001.

E-mail addresses: sakai.nobuo.570@m.kyushu-u.ac.jp, sakai.nobuo@ise.kyutech.ac.jp (N. Sakai), sawa@mech.kyushu-u.ac.jp (Y. Sawae), tmura@mech.kyushu-u.ac.jp (T. Murakami).

articular cartilage is mentioned with sincerely devolving further descriptions on other review papers.

Articular cartilage is a soft tissue containing high water content (70–80% by weight) in an intact state. The high water content is derived from aggregate proteoglycan, which induces osmotic pressure for swelling behavior. Constitutive proteoglycan in the matrix is enmeshed and bound in a fibril network of type II collagen that also functionally reinforces total cartilaginous matrix. The fibril network resists tensile loads in the stress field of the matrix, while proteoglycan (and other quantitative constituents including chondrocyte) mainly takes in charge of supporting compressive load at equilibrium condition. Experimentally, tensile stiffness of articular cartilage is much higher than compressive stiffness of equilibrium condition [3]. Articular cartilage tissue exhibits tension–compression nonlinearity [4,5]. Note that surface constitutions of articular cartilage including gel-like layer, molecular structure on surface and its interaction with synovial fluid lubricants are also employed to enhance reduction of friction force in consideration of boundary lubrication phenomenon [6–11].

It is known that articular cartilage has a constitutive inhomogeneity [12–16] and anisotropy [17,18] from surface to bottom zone. Articular cartilage is briefly divided into 3 characteristic layers along depth direction, whose are called superficial, middle and deep zones. In superficial layer, collagen fibril predominantly lies in parallel to surface plane and concentration of proteoglycan content is lowest within 3 zones. As moving toward middle zone, orientation of collagen fibril tends to be vertical to the surface plane and proteoglycan content rises. In deep zone, collagen fibril is predominantly oriented to vertical to the plane of subchondral bone and proteoglycan content is maintained its concentration as high as that in middle zone. Most bottom of cartilaginous tissue is connected to subchondral bone, called tidemark. Any other constitutive properties of the matrix, which includes density and structure of collagen network, water content, electrical charge, morphology of the cells, etc., vary along depth direction. Consequently, mechanical properties, which are represented as tensile and compressive modulus, permeability of interstitial fluid and so on, also vary along depth direction.

A role of soft material for transmitting loads between articular surfaces is to distribute contact load and consequently reduce the subchondral peak stress. In concerning with articular cartilage, one of the most notable findings on tribological behavior is addressed to the biphasic lubrication mechanism. A fundamental theoretical model of biphasic theory [19] for representing articular cartilage consists of solid phase and fluid phase as a porous media model. When a counter surface contacts to biphasic matrix with some apparent contact area, the fluid content in the tissue is trapped within contact area. Under a load given by counter surface, the collagen network resists interstitial fluid pressure in aggregate solid matrix, and still interstitial fluid cannot flow well in the biphasic matrix due to its low permeability. Then, considerable high pressurization of interstitial fluid occurs under the contact area even in unconfined compression [20]. Thus, the interstitial fluid pressure supports considerable proportion of total load in contact area and this situation consequently causes a reduction of contact force of solid phase. Under an assumption that nonviscous property of fluid phase does not produce friction force, the reduction of the proportion of total contact force on solid phase as a load sharing mechanism subsequently results in low friction coefficient [21]. The biphasic lubrication mechanism has successfully proven the low friction coefficient and time-dependent behavior of articular cartilage by both experimental and theoretical examination past a few decades. Particularly, computational implement for finite element method of biphasic theory advanced predictions of the behavior of cartilaginous tissue

including interstitial fluid pressurization. A linear correlation between interstitial fluid pressurization and resultant behavior on friction coefficient, which had been predicted by theoretical analysis [22], was experimentally confirmed with directly utilizing micro pressure sensing device [23].

Combination of theoretical analyses and corresponding experimental measurements has successfully revealed the important material properties of articular cartilage from the viewpoint of biphasic framework. While more detailed expressions of the constitutions of cartilaginous tissue on theoretical model have advanced to obtain more exact behavior [24–34], one of the recent concerns seems to be a dynamic and physiological condition in terms of mechanical functionality as a load-bearing for articular joint system beyond material testing, which is often conducted in relatively smaller loading speed and magnitude than physiological one. In human body, articular cartilage of lower extremity in walking condition is normally exposed to a cyclic load of several times body weight with rolling and sliding motions. Upon considering these conditions, physiological load levels and contact geometries (conformity of two surfaces) were examined in accounting for the shape of hip and/or knee joint in order to interpret a results from material testing level [35,36]. Compressive reaction force of articular cartilage under physiological cyclic loading was experimentally characterized on frequency response [37]. The effect of physiological cyclic loading on experimental frictional response was examined to test whether a cyclic load maintained the interstitial fluid pressure or not, which offers low friction coefficient [38]. The effect of the soft biphasic amorphous layer on the top surface of cartilaginous tissue was verified by the biphasic finite-element (FE) model under cyclic loadings including the physiological frequency [39]. The mechanical role of the deep vertical fibril was found on the reactional stiffness of spherical indentation especially in the transient period of the physiological condition [40].

One of the tribological factors for a load-bearing is to introduce the sliding motion. By experimental friction tests, Caligaris reported that migrating contact area, which delivers re-swelling periods to the tissue, significantly promoted the sustainability of the interstitial fluid pressurization mechanism and consequent low friction coefficient [41]. Also, Pawaskar introduced the sliding motion into a biphasic FE model and remarked the importance of migrating contact area for sustainability of the biphasic lubrication [42], but the effectiveness of complicated material properties has not been sufficiently evaluated for sliding motion. We thought that physiological loading speed and migrating contact area should be important factors for an integration of mechanical properties of articular cartilage to recognize functionality in actual conditions as a load-bearing in living body. In our present study, the compressive response of the articular cartilage in relatively physiological condition was examined by high precision testing machine with a feedback-controlled servomotor. Material properties of biphasic FE model, which included inhomogeneous apparent Young's modulus of solid phase along depth, strain-dependent permeability and collagen reinforcement in tensile strain, were estimated in cylindrical indentation geometry by a curve fitting between the experimental time-dependent behavior and FE model simulation. Then, by using the modulated FE model, the biphasic lubrication mechanism of articular cartilage including migrating contact area was simulated to elucidate functionality as a load-bearing material.

2. Methods

Both experimental material testing and biphasic FE model analysis were conducted mutually to confirm a part of results. In experimental compressive test, relatively high compressive speeds

with large compressive amplitudes were applied to the tissue to observe the dynamic response for expectantly aiming at more physiological condition. The depth-dependent apparent Young's modulus was experimentally obtained from local strain field at equilibrium state. A cylindrical indenter was adopted in both the experimental compression test and FE analysis to examine the effect of sliding motion of the indenter over cartilage surface. Time-dependent compressive response by cylindrical indenter was used to identify the material properties for consequent FE model analysis. In the FE model analysis with sliding indenter, the effect of migrating contact area was examined with more actual material properties for expressing articulation of cartilaginous tissue.

2.1. Experimental apparatus and materials

The compressive test of cartilaginous tissue has been thought in the past to be difficult to gain accurate results in physiological high-speed compression. In this study a self-made compressive tester shown in Fig. 1 was developed to offer precise motion of compressive platen or indenter. The platen was driven by a ball screw (KR-15, THK) and a servomotor (MR-J2-Jr, Mitsubishi Electronic Corporation) via a load cell (LUR-A-50NSA1, Kyowa electronic instruments). Since a load cell involves its own deformation, which disturbs an accuracy of the position of an end

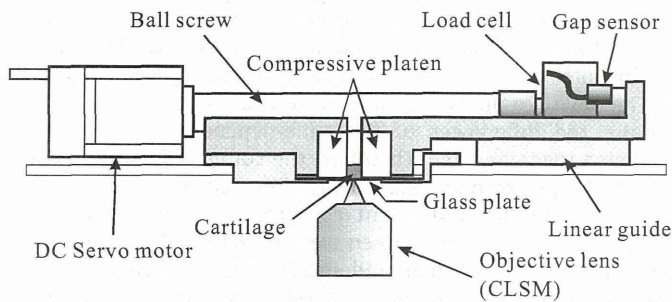


Fig. 1. A schematic drawing of compressive tester for CLSM observation. A feedback control with the displacement sensor (gap sensor using Eddy current) precisely actuated the platen with the position accuracy of 0.5 μm and the maximum speed of 4000 μm/s in any loading condition. The compressive tester was installed on the stage of the CLSM to observe the local strain of the tissue through the glass plate.

effector, the position of the compressive platen was directly detected by Eddy current displacement sensor (E2CA-X1R5A, Omron). A feedback control with the displacement sensor precisely actuated the platen with positional accuracy of 0.5 μm and maximum speed of 4000 μm/s in any loading condition. Sampling rate of overall control loop with a measurement of reaction force was arranged at 333 Hz. The compressive tester was installed on the stage of confocal laser scanning microscope (CLSM, C1-Plus, Nikon Corporation) to observe local strain of the tissue through a glass plate. Both of the compressive platens were made of impermeable alumina ceramics. In compressive test of the cylindrical indenter, additional cylindrical stainless steel with 5 mm radius (SUS316L, impermeable solid) was attached on one of the plate.

Experimental tissue was dissected from distal end of femur in porcine knee (6–8 months old) without any freezing after a processing to prevent change on mechanical properties [43]. For first compressive test on the measurement of depth-dependent strain distribution, a 3 mm cylindrical core with subchondral bone was harvested by a biopsy punch and then split into the half perpendicular to articular surface with a scalpel blade, shown in Fig. 2(a). For the indentation by the cylindrical indenter, a bar shaped osteochondral explant with the dimension of about 2.5 mm width and 10 mm length was dissected by a scalpel blade with preserving intact surface of the tissue, shown in Fig. 2(b). The direction of the longitudinal axis of the bar explant was parallel to physiological anterior–posterior line in the chondyle. The samples were washed by PBS (Phosphate Buffered Saline; pH 7.4, Invitrogen Corporation). Then, living cells as markers for recognizing deformation of solid phase were stained with Calcein-AM (C-3099, Molecular Probes.). The samples were incubated for 30 min staining and washed by PBS again. Compressive tests were examined in PBS solution through the experiment to maintain moisture of the tissue and osmotic phenomenon.

For the compressive test, osteochondral specimen was put on the glass plate and compressed in a condition of unconfined compression. Since the entire specimen in our experiment preserved subchondral bone, the depth of each cartilaginous tissue was acquired prior to the test by measuring the image length from surface to tidemark in microscopic view. Before the compressive test, initial compressive load with 0.05 N of peak load was given for 5 s to make sure of a stable contact. Then, the initial load was removed and the compressive test was immediately executed under the observation of microscopic view. The cartilage

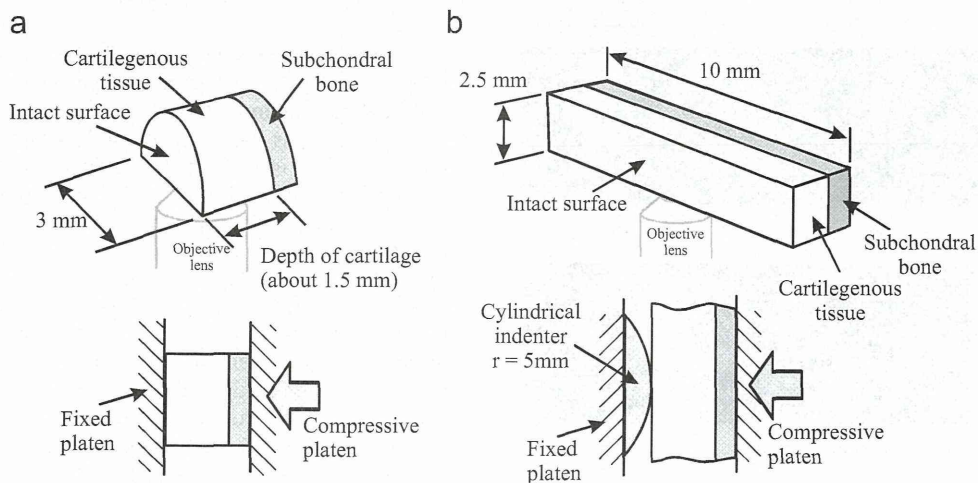


Fig. 2. (a) For the measurement of depth-dependent strain distribution, a 3 mm cylindrical core with subchondral bone was harvested by a biopsy punch and then split into the half perpendicular to the articular surface (Platen compression test). (b) For the indentation by the cylindrical indenter, a bar shaped osteochondral explant with the dimension of about 2.5 mm width and 10 mm length was dissected with preserving the intact surface.

specimen was compressed to the prescribed compressive distance at a constant velocity. Thereafter, the position of the compressive platen or the indenter was kept constant by the feedback position control for a stress relaxation period. During the test, the compressive load or the reaction force was monitored and fluorescence images were acquired as necessary.

2.2. Derivation of depth-dependent Young's modulus from experimental compressive test

The depth-dependent variation of Young's modulus of the solid phase was estimated by the platen compression of half-cylindrical specimen, shown in Fig. 2(a). Content of this section has been partly reported by our previous paper [44]. The specimen was put on the glass plate with facing the cut section of the punched cylindrical explant split half. In this experiment, the total compression of 10% of the depth of cartilaginous tissue and the compressive velocity of 1000 $\mu\text{m/s}$ were employed as primary compressive motion, and then the platen was kept during stress relaxation for 30 min to ensure an equilibrium condition where the interstitial fluid nearly cease flowing. Fluorescent images before compression and at equilibrium condition were obtained by CLSM to estimate the local strain, which represents the variation of apparent compressive Young's modulus of solid phase along depth direction in the correlation of two images. Fig. 3 shows typical fluorescent images before compression and at equilibrium condition. The same cells were carefully identified in both images. In this situation, the local compressive strain ε is easily calculated from the change of the distance between corresponding pair of cells in fluorescent images using Eq. (1), where a and b are the distance of the cell-to-cell before compression and at equilibrium, respectively:

$$\varepsilon = \frac{a-b}{a} \quad (1)$$

The local strain $\varepsilon(x)$ was obtained as the function of depth position x ($0 < x < 1$; the position 0 means surface). Since the interstitial fluid pressure subsides to zero in equilibrium condition, it is considered that only solid phase carries compressive load in biphasic model. Under an assumption of disregarding the lateral deformation, total stress $\sigma_0 = E_0 \varepsilon_0$ as a property of entire specimen is equal to local stress σ in any depth position, where E_0 and ε_0 are total apparent Young's modulus of solid phase and total strain, respectively. The relationship between total stress and

local stress in equilibrium state is given by $E_0 \varepsilon_0 = E(x) \varepsilon(x)$, where $E(x)$ is the depth-dependent Young's modulus. Thus $E(x)$ is given by

$$E(x) = \frac{\varepsilon_0}{\varepsilon(x)} E_0 \quad (2)$$

E_0 and ε_0 can be acquired from a total reaction of the tissue by the compressive testing apparatus and $\varepsilon(x)$ by the microscopic images written before. Note that the small Poisson's ratio of the solid phase in some literatures have been indeed applied or estimated as the value nearly 0 (Jurvelin et al. as 0.158 ± 0.148 , Wilson et al. as 0.15, Warner et al. as 0.08, Graindorge et al. as 0, and Pawaskar et al. as 0.08) [17,32,35,39,42].

2.3. Experimental method for cylindrical indentation

The cylindrical indentation test was conducted to gain time-dependent reaction force for the estimation of constitutive material properties, whose were applied to the following FEM analysis. In this experiment, cylindrical indenter of 5 mm radius was pressed to the bar specimen shaped with about 2.5 mm width and 10 mm length shown in Fig. 2(b). The bar specimen was put on the glass plate of the compressive tester, in which intact surface of the cartilaginous tissue faced to the indenter. We could observe an image of the cutting section through microscope. The image was utilized to measure the depth of the cartilaginous tissue from the osteochondral specimen. In this study, the opposite of the sectional surface facing to the glass plate for microscopic observation was not constrained and the tissue was soaked in PBS during the experiment. Total compressive displacement of the indenter was 10% of the tissue depth at the cylindrical apex of the indenter. Compressive times were chosen as 2, 5, and 10 s to acquire the differences of the time-dependent reaction force including the peak force. Therefore, the compressive speeds were 5%, 2%, 1% per second, respectively. One specimen was sequentially used in the 3 different compressive speeds. After each compression trial, the specimen was soaked in PBS for 30 min to recover its water content and intact shape. Repeatability was checked prior to the experiment; however a disturbance on stable contact seemed equal to the variance of the repeatability. There are some differences in the cylindrical indentation from the platen compression configuration. One of the differences of cylindrical indentation is that the effect of surface seepage of water content should be incorporated into the reaction response.

2.4. Estimation of material properties

Material properties were specified by curve fitting comparing FEM calculation with experimental time-dependent reaction force of the cylindrical indentation. A commercial package ABAQUS (6.8-4), which was past appropriately evaluated for the biphasic analyses [45], was used in this study. Two-dimensional model was accepted to easily introduce consequent sliding motion of the cylindrical indenter shown in Section 2.5. Model geometry for estimating material properties was almost the same to the experimental configuration of the cylindrical indentation written in Section 2.3, shown in Fig. 4. The dimension of the model was 1.5 mm thickness and 10 mm length as a typical shape of the experimental specimens. The metallic cylindrical indenter (stainless steel) was of 5 mm radius represented by geometrical rigid body. The biphasic tissue was modeled by CPE4RP (four-node bilinear displacement and pore pressure, reduced integration with hourglass control) elements and the mesh size was chosen as 0.1 mm^2 . The bottom of the model was fixed and impermeable, where no flow was allowed through the bottom surface. The other surfaces were not fixed and basically permeable except for the

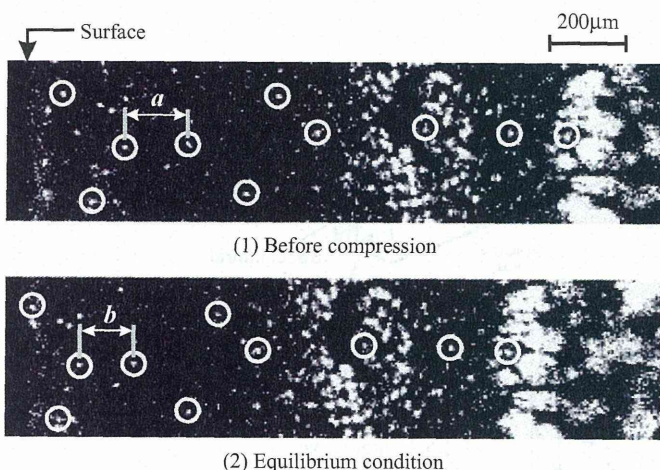


Fig. 3. Typical fluorescent images before compression and at equilibrium condition. The same cells were carefully identified in both images. Since these images were scanned with smallest pinhole of CLSM for an example, the number of cells seems to be small.